The Journal of Chemical Physics

Effect of ligand binding on riboswitch folding: Theory and simulations

Cite as: J. Chem. Phys. **154**, 185101 (2021); https://doi.org/10.1063/5.0047684
Submitted: 16 February 2021 . Accepted: 23 April 2021 . Published Online: 10 May 2021

Shivangi Sharma, Vishal Singh, and Parbati Biswas

The Journal of Chemical Physics ARTICLE scitation.org/journal/jcp

Effect of ligand binding on riboswitch folding: Theory and simulations

Cite as: J. Chem. Phys. 154, 185101 (2021); doi: 10.1063/5.0047684
Submitted: 16 February 2021 • Accepted: 23 April 2021 •
Published Online: 10 May 2021

Shivangi Sharma, Vishal Singh, and Parbati Biswas[a)]

AFFILIATIONS

Department of Chemistry, University of Delhi, Delhi 110007, India

[a)]Author to whom correspondence should be addressed: pbiswas@chemistry.du.ac.in

ABSTRACT

The effect of ligand binding on the conformational transitions of the *add* A-riboswitch in cellular environments is investigated theoretically within the framework of the generalized Langevin equation combined with steered molecular dynamics simulations. Results for the transition path time distribution provide an estimate of the transit times, which are difficult to determine experimentally. The time for the conformational transitions of the riboswitch aptamer is longer for the ligand bound state as compared to that of the unbound one. The transition path time of the riboswitch follows a counterintuitive trend as it decreases with an increase in the barrier height. The mean transition path time of either transitions of the riboswitch in the ligand bound/unbound state increases with an increase in the complexity of the surrounding environment due to the caging effect. The results of the probability density function, transition path time distribution, and mean transition path time obtained from the theory qualitatively agree with those obtained from the simulations and with earlier experimental and theoretical studies.

I. INTRODUCTION

The adenosine deaminase (*add*) A-riboswitch is one among the widely studied class of purine riboswitches[1,2] that is stabilized by ligand binding. These ligand induced conformational transitions transform the folding pattern of the expression platform and affect the folding dynamics of the riboswitch, which in turn influences the cellular processes that controls the expression of proteins. Single molecule force spectroscopy (SMFS) experiments have investigated the hierarchical folding of the *add* A-riboswitch aptamer with adenine binding[3,4] by piecewise integration of all two-state transitions of the riboswitch intermediates obtained from the unfold–fold transitions of the riboswitch aptamer in the optical trap.[4] SMFS measures the extension of the aptamer domain of the riboswitch either through laser tweezers[5,6] or an atomic force microscope (AFM).[7,8] The molecular extension, measured in terms of the end-to-end distance, is chosen as a suitable reaction coordinate to estimate the free energy (potential) profiles of the conformational transitions of the riboswitch aptamers. Experiments reveal that the unfold/fold transition of the *add* A-riboswitch aptamer may be modeled as the stochastic dynamics of this reaction coordinate in an asymmetric free energy landscape.[4,9]

Transition path times obtained from experiments provide essential information about the conformational transitions of the *add* A-riboswitch aptamer across the potential barrier.[10–12] Transition paths of a molecule are defined as the subset of the trajectory where it crosses the barrier top while switching from one conformation to the other across a potential barrier before returning to the initial state.[13–17] These paths contain microscopic information about the unfold/fold reaction mechanisms. Experimental characterization of these transition trajectories poses a formidable challenge due to their very short duration. Most theoretical studies assume a stochastic Markovian dynamics of the reaction coordinate for probing such transition events. However, the anomalous folding dynamics due to the conformational transitions of RNA is non-Markovian as it occurs in a viscoelastic cellular environment.[14,18]

This article presents a transition path time analysis of the anomalous folding dynamics associated with the conformational transitions of the *add* A-riboswitch aptamer within the framework of Generalized Langevin Equation (GLE) with correlated thermal fluctuations in a viscoelastic cellular environment. Steered Molecular Dynamics (SMD) simulations are also performed to probe the effect of ligand binding on the conformational transitions of the riboswitch aptamer. Theoretical and simulation results provide a qualitative

estimate of the typical transit times along with the exact shape of such distributions, which is difficult to determine experimentally. The results of the probability density function, transition path time distribution (TPTD), and mean transition path time (MTPT) of the riboswitch aptamer obtained from both theory and simulation qualitatively agree with each other and with those of SMFS experiments.

II. THEORY

The adenosine deaminase (*add*) A-riboswitch aptamer is one among the widely studied class of riboswitches that regulates the purine metabolism. The secondary structure of its aptamer domain has a three-way tuning fork structure, which involves three RNA helices as *P*1, *P*2, and *P*3 with two hairpin loops as *L*2 and *L*3,[1,2,4] given in Fig. 1(a). The hierarchical folding of the riboswitch may be viewed as an assembly of multiple distinct two-state processes, which governs the unfold/fold transition of the riboswitch across a barrier between two wells in the potential energy landscape. The two asymmetric wells correspond to the energy of the fully folded (*F*) and *P*1 unfolded (*P*1_*U*) states of the riboswitch both with and without the ligand (adenine). The dynamics of ligand binding induced unfold/fold transition of the *add* A-riboswitch aptamer in a viscoelastic cellular environment may be theoretically modeled in terms of one-dimensional diffusion in the potential energy landscape. SMFS experiments establish the unfold transition of the *add* A-riboswitch aptamer as $F \rightarrow P1\_U \rightarrow P2/P3 \rightarrow P3 \rightarrow U$, while the folding mechanism follows a reverse order.[4,9] A schematic diagram of the energy landscape pathway of the aptamer folding in the absence (black) and in the presence (red) of adenine is shown in Fig. 1(c). The presence of numerous tertiary contacts among the conserved bases at the three-way junction is responsible for direct binding of the ligand to the aptamer. The adenine ligand binding stabilizes the triple helix junction of the aptamer domain by enhancing the secondary and/or tertiary interactions [refer to Fig. 1(b)], which increases the force required to unfold the fully folded aptamer. Thus, the population of the other intermediate states is reduced, and the *P*2/*P*3 states are often not observed. These experimental findings confirm that ligand binding governs the two-state transition between the *P*1_*U* and the fully folded state *F* (i.e., $F \rightarrow P1\_U$ or $P1\_U \rightarrow F$), which is the rate limiting step in riboswitch folding.[9]

The trajectories of each of these unfold/fold transitions are experimentally determined via the changes in the extensions of the riboswitch aptamers as it unfolds or folds via gradual increase/decrease in the applied force. These transitions are quantified by the reaction coordinate, *x*. The time evolution of this reaction coordinate that determines the fold–unfold transitions of the *add* A-riboswitch aptamer between its fully folded (*F*) and *P*1 unfolded (*P*1_*U*) state, both in the absence and presence of ligands in viscoelastic cellular environments, may be studied within the framework of the overdamped generalized Langevin equation,[19,20]

$$m \int_0^t \gamma(t-t')\, \dot{x}(t')\, dt' = -\frac{dU(x)}{dx} + \xi(t), \tag{1}$$

where $x(t)$ is the time dependent extension of the *add* A-riboswitch aptamer, which represents the reaction coordinate, and $U(x)$ denotes the effective potential (free energy) of unfold/fold transitions of the riboswitch aptamer between the fully folded (*F*) and *P*1 unfolded (*P*1_*U*) state. Here, $\xi(t)$ represents the correlated thermal fluctuations imparted by the surrounding cellular environment with zero mean, $\langle \xi(t) \rangle = 0$, which is related to the frictional memory kernel $\gamma(t)$ by the fluctuation–dissipation theorem. The structural rearrangement of the *add* A-riboswitch aptamer with and without ligand (adenine) binding between the fully folded and *P*1 unfolded state is characterized by the stochastic dynamics of the reaction coordinate (molecular extension) in an asymmetric bistable potential well.[1,4,9] The potential energy curves obtained from SMFS experiments suggest that the two states (i.e., *F* and *P*1_*U*) of the riboswitch aptamer are of unequal energy. However, when the riboswitch aptamer

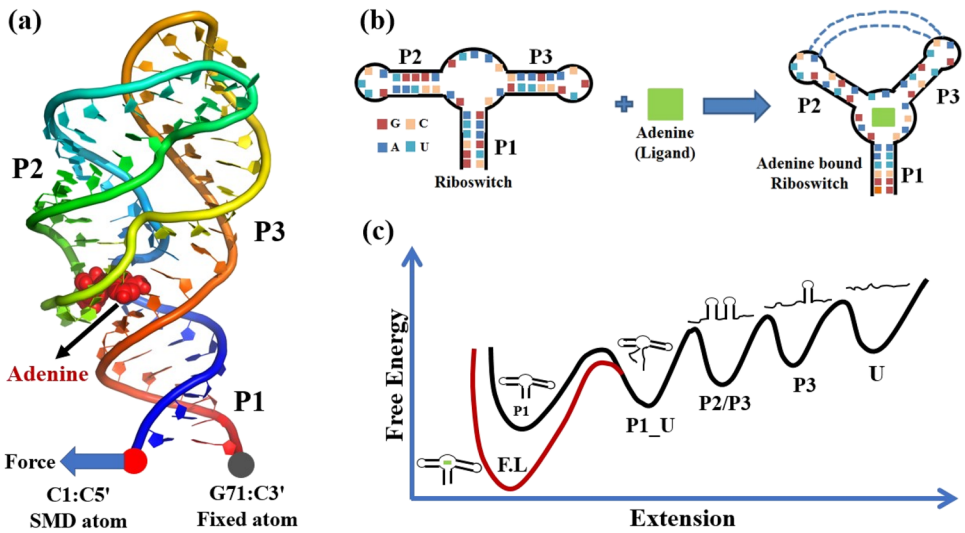

FIG. 1. (a) The tertiary structure (PDB ID: 1Y26) and (b) secondary structure representation of the *add* A-riboswitch aptamer. The blue dashed lines show the loop–loop interaction in response to the ligand (adenine) binding. (c) A schematic representation of the energy landscape of the aptamer in the presence (denoted by red line) and absence (denoted by black line) of the ligand binding.

(i.e., $F \bullet L$) binds to a ligand, it stabilizes the fully folded state further due to an increase in the secondary and tertiary interactions, which increases the corresponding force required to unfold the fully folded state. Hence, the free energy of the fully folded state (F) of the riboswitch with the ligand (L) is additionally stabilized by −8 kcal/mol as compared to that without the ligand.[1] Thus, the potential energy landscape corresponds to an asymmetric bistable well with an increased well depth for the $F \bullet L$ state.[21]

The asymmetric bistable potential for the *add* A-riboswitch aptamer for both ligand bound and unbound states may be mathematically modeled through a generalized asymmetric double-well potential[22,23] with a biasing parameter, ($\mathcal{B}$). The algebraic expression may be expressed as a linear combination of the odd and even solutions of the Weber equation.[24] Analytically, an asymmetric double-well potential for the conformational transition of the riboswitch aptamer may be represented as

$$U(x) = 2k_BT \ln \Phi(A, x), \tag{2}$$

where

$$\begin{aligned}\Phi(A,x) &= y_1(A,x) + \mathcal{B}\, y_2(A,x)\\ &= \exp\left(-\frac{k_S\, x^2}{4k_BT}\right)\left[{}_1F_1\left(\frac{A}{2}+\frac{1}{4},\frac{1}{2};\frac{k_S}{2k_BT}x^2\right)\right.\\ &\quad \left. + \mathcal{B}\, x\sqrt{\frac{k_S}{k_BT}}\,{}_1F_1\left(\frac{A}{2}+\frac{3}{4},\frac{3}{2};\frac{k_S}{2k_BT}x^2\right)\right],\end{aligned} \tag{3}$$

where $-1/2 \le A < 0$ and

$$\mathcal{B} < \mathcal{B}_c = \sqrt{2}\,\frac{\Gamma(A/2+3/4)}{\Gamma(A/2+1/4)}.$$

Here, ${}_1F_1(\alpha, \beta; z)$ represents the confluent hypergeometric function,[25] and k_S is the curvature of the potential barrier or the stiffness of the optical trap.[10,26] Different values of the parameter A; $-1/2 \le A < 0$ correspond to the depth of the bistable potential well. The biasing parameter, $\mathcal{B}$, dictates the extent of asymmetry in the double-well such that $\mathcal{B} < \mathcal{B}_c$, where $\mathcal{B} > 0$ denotes an increase in the depth of the left potential well as compared to the right one, and vice versa for $\mathcal{B} < 0$. However, for $\mathcal{B} = 0$, the potential corresponds to a perfectly symmetric bistable potential well.

The structural transitions of the riboswitch aptamer with and without ligand binding occur in a viscoelastic cellular environment, which is governed by long-time correlated thermal fluctuations that determine the extent of the interactions between the riboswitch and the surroundings.[27] The heterogeneity of the surroundings introduces memory effects in the system, which accounts for the non-Markovian behavior with an anomalous dynamics.[27–29] This anomalous conformational dynamics of the *add* A-riboswitch aptamer may be modeled through power-law correlated thermal fluctuations as

$$\langle \xi(t)\xi(t')\rangle = \frac{k_BT\eta_\beta(|t-t'|)^{-\beta}}{\Gamma(1-\beta)}. \tag{4}$$

Here, η_β represents the fractional friction coefficient, which may be defined as $\eta_\beta = \eta/\tau_c^{(1-\beta)}$, where τ_c is the correlation time and Γ is the Gamma function. The scaling exponent β, with $0 < \beta \le 1$, determines the degree of the heterogeneity of the surrounding environment, where $\beta = 0$ denotes a completely heterogeneous environment and $\beta = 1$ corresponds to a completely homogeneous (diffusive) surrounding. Equation (4) may also be written as

$$\langle \xi(t)\xi(0)\rangle = \frac{k_BT\eta_\beta t^{-\beta}}{\Gamma(1-\beta)}. \tag{5}$$

The analysis of the transition path time (TPT) for the conformational transition of the *add* A-riboswitch aptamer requires the probability density, $P(x, t)$, which denotes the probability of finding the reaction coordinate x of the riboswitch in an asymmetric potential energy landscape at time t. The overdamped GLE in Eq. (1) is solved for the asymmetric potential in Eq. (2) with power-law thermal fluctuations as given by Eq. (4). The characteristic non-Markovian dynamics of the system transforms the probability, $P(x, t)$, in terms of the conditional probability distribution function, $P(x, t|x_0)$,[19,20,27] that may be defined as the conditional probability of finding the reaction coordinate x of the riboswitch aptamer at time t in the potential well, given that it is located at x_0 at an initial time $t = 0$. Thus, the Fokker–Planck equation is transformed to an effective Fokker–Planck equation (EFPE), which may be expressed in terms of the conditional probability distribution function (refer to Secs. A–E of the supplementary material) as[27]

$$\frac{\partial P(x,t|x_0)}{\partial t} = D(t)\left[\frac{\partial^2}{\partial x^2} + \frac{\partial}{\partial x}\frac{U'(x)}{k_BT}\right]P(x,t|x_0). \tag{6}$$

Here, $U(x)$ represents an asymmetric bistable potential, while the prime $'$ denotes the derivative with respect to the reaction coordinate x. $D(t)$ is the time dependent diffusion coefficient of the riboswitch aptamer in the viscoelastic cellular environments, which may be obtained as (refer to Sec. A of the supplementary material)

$$D(t) = \frac{k_BT}{k_S}\frac{\dot{\mathcal{Z}}(t)}{\mathcal{Z}(t)}, \quad \text{where} \quad \mathcal{Z}(t) = E_{\beta,1}\left(\frac{k_S}{\eta_\beta}\,t^\beta\right), \tag{7}$$

where $E_{a,b}$ represents the two-parameter Mittag–Leffler function and[30] $\mathcal{Z}(t)$ may be written as

$$\mathcal{Z}(t) = E_{\beta,1}\left(D_\beta\frac{k_S}{k_BT}\,t^\beta\right), \tag{8}$$

where $D_\beta = \left(\frac{k_BT}{\eta_\beta}\right)\text{nm}^2\mu\text{s}^{-\beta}$, and for $\beta = 1$, $D_1 = \left(\frac{k_BT}{\eta}\right)\text{nm}^2\mu\text{s}^{-1}$ such that D_1 represents the diffusion coefficient[11] for the structural transition of the *add* A-riboswitch aptamer in an asymmetric bistable potential under normal diffusive conditions in completely homogeneous surroundings. However, D_β represents the diffusion coefficient in the viscoelastic cellular environment, both in the absence and presence of the ligand (adenine). The scaling exponent β determines the degree of heterogeneity of the surroundings, with $0 < \beta \le 1$. The ratio of the two diffusion coefficients is $0 < \frac{D_\beta}{D_1} \le 1$, which confirms the retarded structural motion of the riboswitch aptamer in cellular environments as compared to its motion in the homogeneous surroundings. The values of the diffusion coefficients that characterize the structural transitions of the riboswitch aptamer are obtained from the experiments of Neupane *et al.*,[11] which involve

the reconstruction of the folding energy landscape profiles from the extension trajectories at constant force with the removal of instrumental compliance effects by deconvolution. The typical values of these diffusion coefficients reported for the conformational transitions of the *add* A-riboswitch aptamer in a normal diffusive environment are given as $D_1 = 0.2\ \text{nm}^2\ \mu\text{s}^{-1}$ and $D_1 = 0.02\ \text{nm}^2\ \mu\text{s}^{-1}$ without and with ligand binding,[11] respectively.

The solution of Eq. (6) in an asymmetric potential, $U(x)$, may be calculated via eigenfunction expansion in spatial and temporal domains as $P(x, t|x_0) = X(x)X(x_0)\tau(t)$, where the bilinear expansion of $P(x, t|x_0)$ may be expressed as (derived in Sec. C of the supplementary material)

$$P(x,t|x_0) = \frac{P_s^{1/2}(x)}{P_s^{1/2}(x_0)}\psi_0(x)\psi_0(x_0) + \sum_{n=0}^{\infty}\frac{P_s^{1/2}(x)}{P_s^{1/2}(x_0)}\psi_{n+1}(x) \times \psi_{n+1}(x_0)\exp\left(-\lambda_{n+1}\int_0^t D(t')\,dt'\right), \tag{9}$$

where $\psi_n(x)$ and λ_n denote the eigenfunctions and the eigenvalues with $P_s(x)$ as the stationary solution of Eq. (6). The final expression of $P(x, t|x_0)$ in an asymmetric potential given by Eq. (2) with the power-law correlated thermal forces defined by Eq. (4) may be obtained by substituting the respective eigenfunctions from Eqs. (S43) and (S52) given in Secs. D and E of the supplementary material, respectively. The temporal solution of Eq. (9) may be given by

$$P(x,t|x_0) = C_0^2\sqrt{\frac{k_S}{k_BT}}\frac{1}{(\Phi(A,x))^2} + \sum_{n=0}^{\infty}C_{n+1}^2\sqrt{\frac{k_BT}{k_S}}(\Phi(A,x_0))^2 \times \frac{d}{dx}\frac{D_n(x)}{\Phi(A,x)}\frac{d}{dx_0}\frac{D_n(x_0)}{\Phi(A,x_0)}\mathcal{Z}(t)^{-\left(n+A+\frac{1}{2}\right)}, \tag{10}$$

where the respective values of the functions $P_s(x)$, $\psi_0(x)$, $\psi_{n+1}(x)$, C_0, and C_{n+1} in Eq. (10) are obtained from Eqs. (S27), (S40), (S41), (S51), and (S57) respectively (derived in Secs. C–E of the supplementary material).

Here, $D_n(x)$ is the parabolic cylinder function,[31,32] defined as $D_n(x) = 2^{-n/2}\exp\left(-ax^2/2\right)H_n(x\sqrt{a})$, and $H_n(x)$ is the Hermite polynomial.[31,32] The normalization constants of the ground and excited states are denoted by $C_0^2 = \left(\frac{\mathcal{B}_c^2-\mathcal{B}^2}{2\,\mathcal{B}_c}\right)$ and $C_{n+1}^2 = \frac{1}{\sqrt{2\pi}n!\left(n+A+\frac{1}{2}\right)}$, $n \geq 0$, respectively (derived in Secs. D and E of the supplementary material). The eigenvalues calculated for the ground and the excited states are represented as

$$\lambda_0 = 0 \tag{11}$$

and

$$\lambda_{n+1} = \sqrt{\frac{k_BT}{k_S}}\left(n + A + \frac{1}{2}\right),\ n = 0, 1, 2\ldots. \tag{12}$$

The solution of Eq. (9) in the temporal domain obtained by substituting $D(t)$ from Eq. (7) and λ_{n+1} from the above equation is given by

$$\tau(t) = \mathcal{Z}(t)^{-\left(n+A+\frac{1}{2}\right)}. \tag{13}$$

The transition path time (TPT)[13,33] is the time required by the riboswitch aptamer with an initial reaction coordinate x_A (or x_B) to reach the final state with the reaction coordinate x_B (or x_A) across the potential barrier via the transition state x_{TS} at the barrier top. A schematic diagram of the transition paths[13,33] corresponding to each of the unfold/fold transitions of the *add* A-riboswitch aptamer within $x_{A_1} < x_{TS} < x_{B_1}$ is depicted in Fig. S1 of the supplementary material. The trajectory begins at x_{A_1} and terminates at x_{B_1} without revisiting its initial position, x_{A_1}, or vice versa. Absorbing boundary conditions at x_{A_1} and x_{B_1} model the unfold/fold transitions at x_{A_1} and x_{B_1} and ensure that the initial states are not revisited. The transition path is defined as the part of the trajectory that originates at x_{A_1} and ends at x_{B_1} within the transition region $x_{A_1} < x_{TS} < x_{B_1}$ and continuously spans the barrier top without being absorbed at the confined boundaries (refer to Fig. S1).[15,16,33–36,39] The generalized expression of the potential, $U(x)$, given by Eq. (2) may be defined for definite values of $A = -1/2$ and $\mathcal{B} = 0$. Thus, the parabolic potential may be represented by

$$U(x)\Big|_{A=-\frac{1}{2}} = 2k_BT\ \ln\ \exp\left(-\frac{k_S}{k_BT}\frac{x^2}{2}\right) = -\frac{k_S\,x^2}{2}. \tag{14}$$

Hence, the characteristic TPTD, $\mathcal{P}_{TPT}(t)$ for the conformational transition of the *add* A-riboswitch in the region $x_{A_1} < x < x_{B_1}$ may be obtained from Eq. (14) as[15,33,34,37–41]

$$\mathcal{P}_{TPT}(t) = -\frac{d}{dt}\int_{x_{A_1}}^{x_{B_1}} P(x,t|x_0)\Big|_{A=-\frac{1}{2}}\,dx, \tag{15}$$

where the conditional probability distribution $P(x, t|x_0)$ in an asymmetric potential may be calculated from Eq. (10) for $A = -1/2$ and $\mathcal{B} = 0$.

MTPT,[13,16,36] $\bar{\tau}_{TPT}$, is a measure of the average time required for a transition between the two conformations of the riboswitch aptamer located at x_{A_1} (or x_{B_1}) and x_{B_1} (or x_{A_1}) across the parabolic potential barrier. Analytically, it may be expressed as $\bar{\tau}_{TPT} = \int_0^\infty t\ \mathcal{P}_{TPT}(t)|_{A=-1/2}dt$. Thus, the MTPT of the conformational transitions of the aptamer in a heterogeneous cellular environment may be expressed as

$$\bar{\tau}_{TPT} = \sum_{n=1}^{\infty}\frac{2^{-n}}{\sqrt{\pi}}\frac{\Gamma(1+\beta)}{nn!}\left(\frac{k_BT}{k_SD_\beta}\right)^{\frac{1}{\beta}}\exp\left(-\frac{\Delta E}{k_BT}\right) \times H_{n-1}\left(\sqrt{\frac{\Delta E}{k_BT}}\right)H_n\left(\sqrt{\frac{k_S}{2k_BT}}x\right)\Bigg|_{x_{A_1}}^{x_{B_1}}, \tag{16}$$

where

$$\frac{\Delta E}{k_BT} = \frac{k_S\,x_0^2}{2k_BT}, \tag{17}$$

where the non-trivial solutions of the above equation exist only for $n \geq 1$. Equation (17) depicts a linear relation between the dimensionless barrier height (or barrier energy) with the curvature of the potential barrier.[27,33]

III. SIMULATION DETAILS

Implicit Steered Molecular Dynamics (SMD) simulations are performed to study the effect of ligand binding on the dynamics

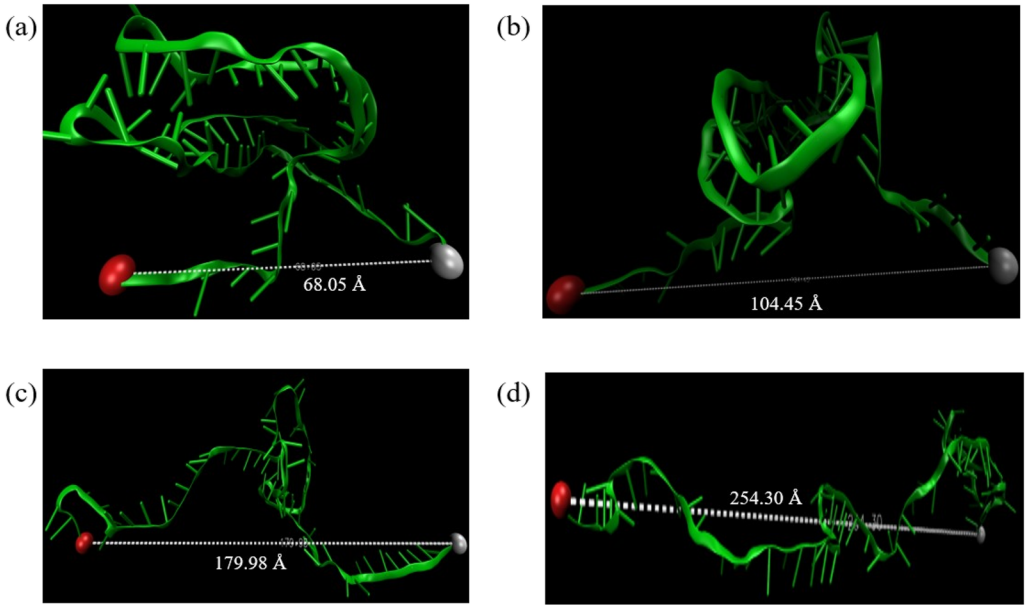

FIG. 2. Snapshots of the unfolding events of the riboswitch aptamer in the presence of the ligand from SMD simulation with a pulling force 10 pN. The end-to-end distances between *C*3′ (gray) and *C*5′ (red) atoms are (a) 68.05, (b) 104.45, (c) 179.98, and (d) 254.30 Å, respectively. Multimedia view: https://doi.org/10.1063/5.0047684.1

of conformational transitions of the riboswitch aptamer. The initial crystal structure of the *add* A-riboswitch aptamer (with ligand) is taken from the RCSB PDB (Research Collaboratory for Structural Bioinformatics Protein Data Bank) with PDBID: 1Y26 [refer to Fig. 1(a)]. The ligand adenine is removed manually to obtain the initial template without the ligand. The SMD simulations are carried out with the NAMD-2.14 suite[42] of programs using AMBER ff99bsc0 and χOL3 force field[43,44] for the nucleic acid. The energy of the system is minimized for 2000 steps to remove all unfavorable interactions. The crystal structure of the riboswitch is also refined during the minimization process. The temperature of the system is gradually increased upto 300 K. The system is equilibrated for 5

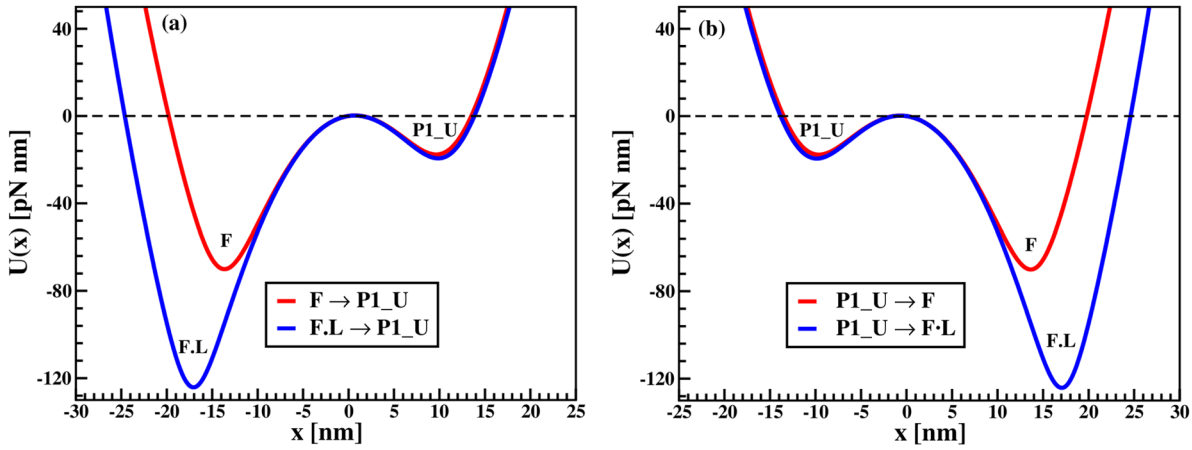

FIG. 3. Asymmetric bistable potential, $U(x)$, as a function of reaction coordinate, x, of the *add* A-riboswitch aptamer with and without ligand binding as obtained from Eq. (2), reconstructed for the experimentally determined potential. Plots (a) and (b) represent the unfold and fold transitions of the riboswitch aptamer between folded (F) and $P1$ unfolded ($P1\_U$) states. Potential energy minimum for $P1$ unfold and fold transition without the ligand corresponds to 10 kcal/mol = 69.20 pN nm obtained for $A = -0.43$, $\mathcal{B} = 0.073$, and with $A = -0.43$, $\mathcal{B} = -0.073$, k_BT = 10 kJ/mol, respectively. Potential energy for $P1$ unfold and fold transition with the ligand corresponds to 18 kcal/mol = 124.56 pN nm for $A = -0.44$, $\mathcal{B} = 0.0717$ and with $A = -0.44$, $\mathcal{B} = -0.0717$, k_BT = 10 kJ/mol, respectively.

ns without any periodic boundary conditions. The Born radius cut-off for each atom is set to 12 Å. The equilibrated aptamer is then subjected to the final production run. The temperature is kept constant throughout the simulation using a Langevin thermostat[45] with a collision frequency $\gamma = 25.0\ ps^{-1}$.

To mimic the SMFS experiment, constant force SMD simulations (with and without the ligand) are performed, where the $C3'$ atom of the $G71$ residue is fixed and a constant force is applied to the $C5'$ atom of the $C1$ residue of the riboswitch aptamer to unfold the RNA completely. Several constant force pulling SMD simulations are performed at different forces (such as 9, 10, 11, 12, 13, and 14 pN) for both ligand (adenine) bound and unbound states of the aptamer. The extension (i.e., the end-to-end distance between $C3'$ and $C5'$ atoms of the riboswitch aptamer) as a function of the simulation time, potential of mean force (PMF), and probability density of the unfolding process of the riboswitch aptamer (with and without ligand) at different constant forces is shown in Figs. S3–S5 of the supplementary material. Snapshots of the unfolding events of the riboswitch aptamer compiled from SMD simulations with a pulling force of 10 pN in the presence and absence of the ligand are shown in Fig. 2 (Multimedia view) and Fig. S9 (Multimedia view) of the supplementary material, respectively.

The structure of the *add* A-riboswitch contains Mg^{2+} ions, which play an important role in the stabilization of the riboswitch aptamer.[46,47] Therefore, SMD simulations with explicit Mg^{2+} ions are also performed to probe the effect of this ion on the unfolding of the riboswitch aptamer both with and without the ligand.

IV. RESULTS AND DISCUSSIONS

Figure 3 represents the asymmetric bistable potential represented by Eq. (2), which models the conformational transitions of the *add* A-riboswitch aptamer between F and $P1\_U$. Figures 3(a) and 3(b) portray the unfold/fold transitions of the $P1$ helix of the riboswitch aptamer, respectively. From experiments, the free energy of unfolding of the $P1$ helix is estimated to be 10 ± 1 kcal/mol without ligand binding, while the energy is 18 ± 2 kcal/mol[1] on ligand binding. Specific values of the parameters are chosen in Eq. (2) to match the results of the theory with those of the experiments. The asymmetric potential with $A = -0.43$, $k_BT = 10$ kJ/mol is considered for the ligand bound transition of the riboswitch aptamer such that $\mathcal{B} = 0.073$ defines the unfolding transition ($F \rightarrow P1\_U$) and $\mathcal{B} = -0.073$ depicts the folding one ($P1\_U \rightarrow F$). Similarly, the unfold and fold transitions of the $P1$ helix with ligand binding is characterized by $\mathcal{B} = 0.0717$ and $\mathcal{B} = -0.0717$, respectively, for $A = -0.44$ and $k_BT = 10$ kJ/mol.

Figures 4(a) and 4(b) depict a comparison of the PMF profile vs scaled extension obtained from the SMD simulation at 10 pN (as shown in an earlier study[9]) and theory from Eq. (2) for both without and with ligand binding of the riboswitch aptamer, respectively. The PMF profile of the folded state matches with the asymmetric

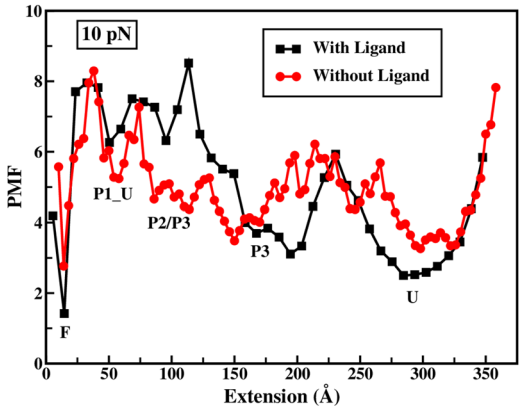

FIG. 5. Comparison of the potential of mean force (PMF) of the conformational transitions of the riboswitch aptamer without and with ligand binding from SMD simulations at 10 pN.

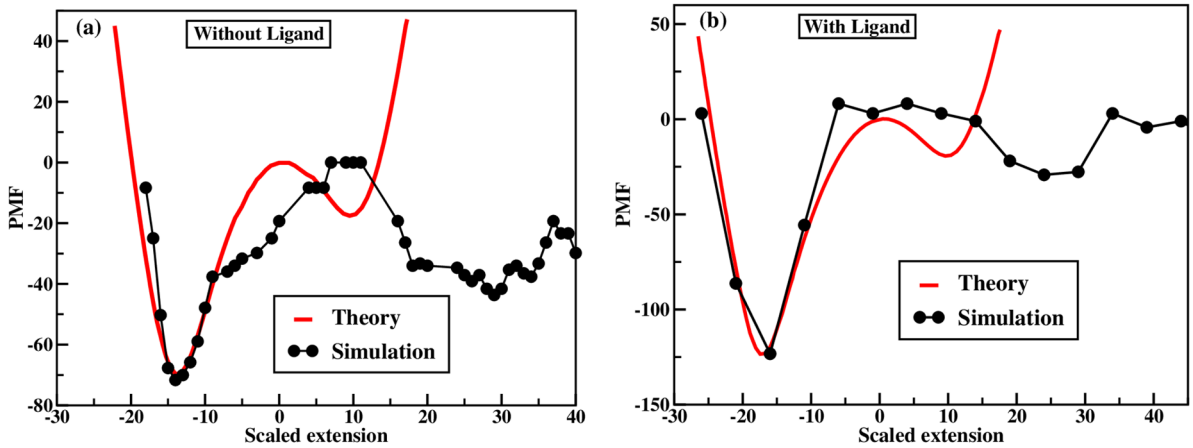

FIG. 4. Comparison of the potential of mean force (PMF) from SMD simulation denoted by a black line and Eq. (2) denoted by a red line for the conformational transition of the riboswitch aptamer (a) without and (b) with ligand binding.

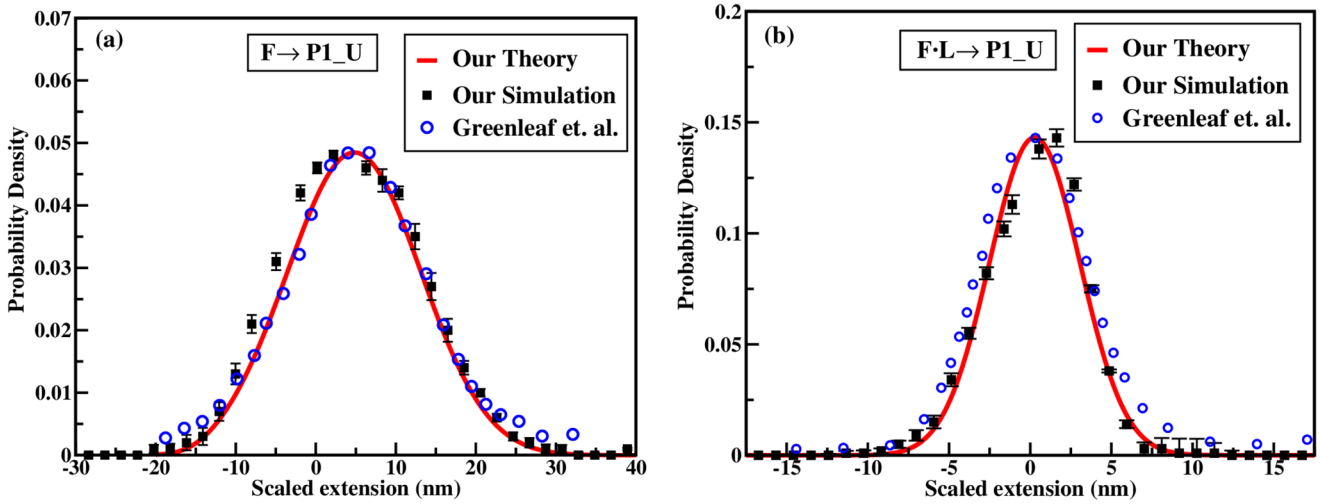

FIG. 6. Comparison of probability density for the unfold transition of the riboswitch aptamer, obtained from our theory [in Eq. (10), by line] and simulation (for constant force at 5.5 pN, by squares), with those of the experiments[4] (by circles). Plot (a) and (b) represent the riboswitch aptamer transition without and with ligand binding, respectively. The error bars are calculated from ten independent SMD simulation trajectories.

bistable potential [from Eq. (2)], but it shows a deviation for the *P*1_*U* state. Broad PMF profiles are observed in simulations as compared to those obtained from the theory as the former accounts for several intermediate conformations along the transition pathway. The choice of the force field also influences the results of the PMF profiles. Figure 5 shows the full PMF profiles of the conformational transitions of the riboswitch aptamer (with and without ligand) for 10 pN, and for different forces, this is shown in Fig. S4 of the supplementary material. Figures S6(a) and S6(b) of the supplementary material show a comparison of the PMF profiles vs extension for implicit and explicit Mg^{2+} ions from the SMD simulations at 10 pN for the unfolding of the riboswitch aptamer, both without and with ligand binding, respectively. The simulations with explicit Mg^{2+} ions further stabilize the folded state of the riboswitch aptamer both without and with ligand binding by increasing the height of the kinetic barrier.[46,47] However, the position of the transition state for the unfolding of the aptamer along the reaction coordinate remains the same for both type of simulations with implicit and explicit Mg^{2+} ions. These findings suggest that explicit Mg^{2+} ions enhance the stabilizing effect of the folded state of the aptamer, which decreases the unfolding rate and increases the folding rate as compared to those with implicit Mg^{2+} ions.[46]

The results of the probability distribution as obtained from Eq. (10) reveal that the unfold–fold transitions are faster and more

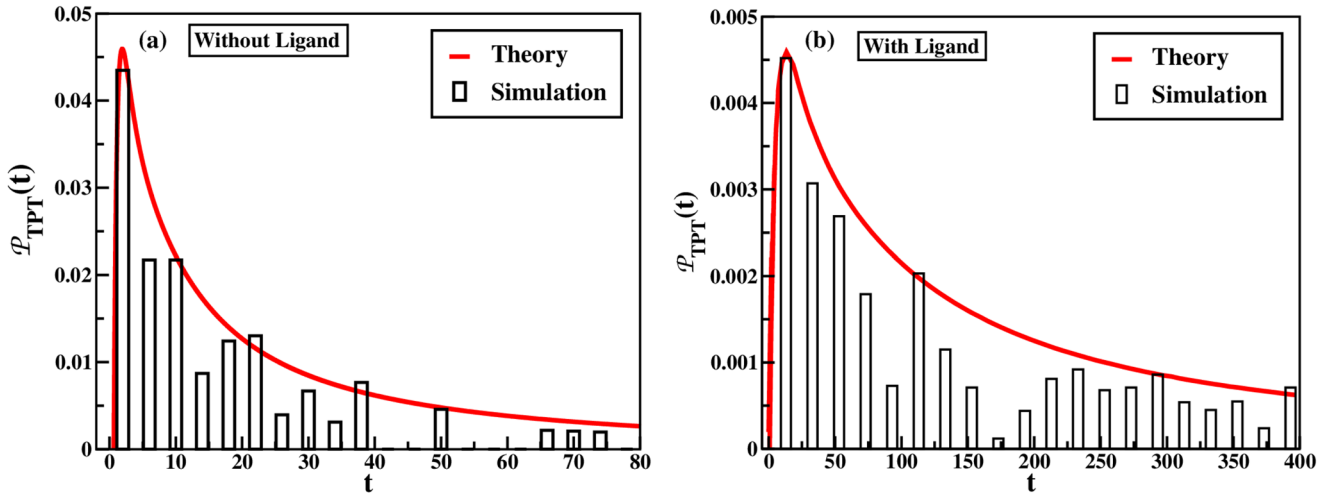

FIG. 7. Comparison of $\mathcal{P}_{TPT}(t)$ vs t for the conformational transition of the riboswitch aptamer (a) without and (b) with ligand binding obtained from our theory [Eq. (15), for $\beta = 1$] with those of simulation. The solid line denotes the theory, and bars denote the simulation.

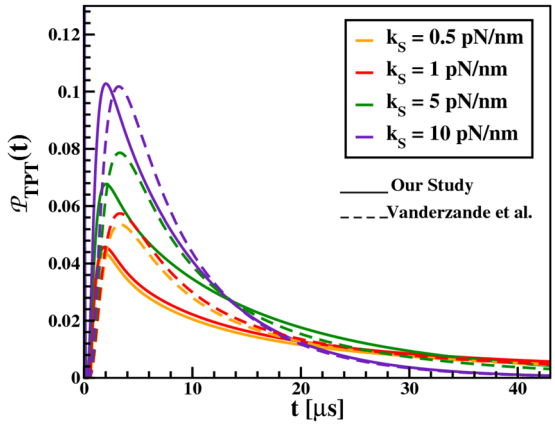

FIG. 8. $\mathcal{P}_{TPT}(t)$ vs t for different barrier heights obtained from Eq. (15). Different curves correspond to varied barrier heights indicated by different k_S values; as k_S = 0.5, k_S = 1, k_S = 5, and k_S = 10 pN/nm for β = 1.

probable as compared to the fold–unfold transitions, as shown in Fig. S2 of the supplementary material. The probability density function of all conformational transitions of the riboswitch aptamer both without and with ligand binding from SMD simulation at different forces is shown in Fig. S5 of the supplementary material.

A comparison of the probability density of the unfolding transition of the riboswitch aptamer vs the scaled extension, x, obtained from the theory [in Eq. (10)] and simulations with those of experiments is shown in Fig. 6. The unfolding of $P1$ helix from the fully folded (F) to the $P1$ unfolded state ($P1\_U$) is the rate determining step.[9] Figure 6(a) depicts the probability density of the aptamer without the ligand for the parameters D_1 = 0.2 nm^2/μs, A = −0.43, $\mathcal{B}$ = 0.073, and k_S = 1 pN/nm. However, Fig. 6(b) portrays the effect of ligand (adenine) binding on the riboswitch with the parameters D_1 = 0.02 nm^2/μs, A = −0.44, $\mathcal{B}$ = 0.0717, and k_S = 0.25 pN/nm. The results of our calculations both from theory and simulations qualitatively agree with the experiments of Greenleaf *et al.*[4]

Figure S7 of the supplementary material depicts the TPTD, $\mathcal{P}_{TPT}(t)$, for the conformational transition of the riboswitch aptamer both without and with the ligand as a function of time, t, for different values of β. The amplitude of the TPTD peaks decrease with a decrease in the values of β. Lower β values correspond to higher viscoelasticity, which retards the motion of the riboswitch aptamer and consequently increases the TPT to cross the barrier. For the conformational transition of the riboswitch with the ligand, the TPT is longer as compared to that without the ligand as the ligand bound structure of the aptamer is more stable. Figures 7(a) and 7(b) show a comparison of the TPTD, $\mathcal{P}_{TPT}(t)$, for the conformational transition of the aptamer both without and with ligand binding, respectively, obtained from our theory [Eq. (15), for β = 1] with those of the constant force SMD simulations (at 10 pN). The results of the theory agree with those of the SMD simulations for both without and with ligand binding of the riboswitch.

Figure 8 represents $\mathcal{P}_{TPT}(t)$ vs time for the conformational transitions of the riboswitch aptamer as calculated from Eq. (15) for different heights of the potential barrier that may be obtained from the values of the stiffness parameter k_S. These different values are k_S = 0.5, k_S = 1, k_S = 5, and k_S = 10 pN/nm (where an increase in k_S denotes an increase in the barrier height). A change in the values of either k_S or x_0 (i.e., change in k_S with x_0 constant or vice versa) generates a potential barrier with varied curvatures,[27,33] as $\frac{\Delta E}{k_B T} = \frac{k_S x_0^2}{2 k_B T}$ [from Eq. (17)]. The results elucidate that the TPT of the transition decreases with an increase in the barrier height. A

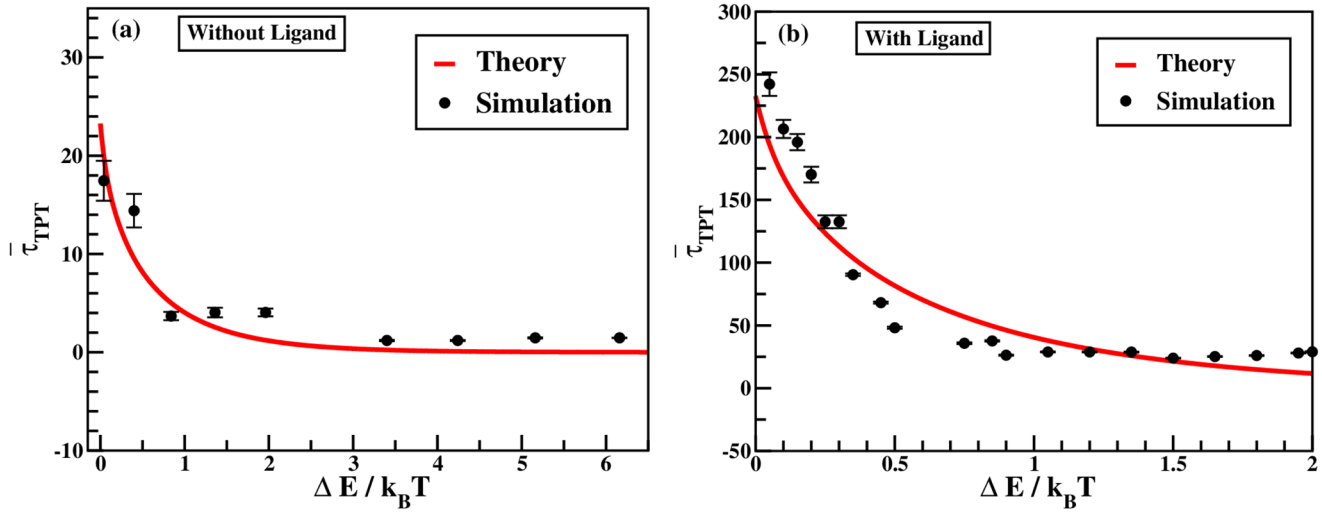

FIG. 9. Comparison of $\bar{\tau}_{TPT}$ for the conformational transition of the riboswitch aptamer (a) without and (b) with ligand binding obtained from our theory [Eq. (16), for β = 1] with those of simulation. The solid line denotes the theory, and circles denote the simulation. The error bars show the standard errors averaged over the mean time of crossing between the two boundaries.

comparison of the results of the TPT distributions obtained from our theory (denoted by solid lines) for absorbing boundary conditions with that of Carlon *et al.*[48] (denoted by dashed lines) for free boundary conditions depicts that the distributions of TPTs for two different boundary conditions overlap with each other with an increase in the height of the barrier. This shows that for higher barrier heights, the TPT distributions remain unaffected by the choice of boundary conditions.[33,49]

Figure S8 of the supplementary material represents the log–log plots of MTPT, $\bar{\tau}_{TPT}$, for the unfold/fold transitions of the *add* A-riboswitch aptamer both in the absence and presence of the ligand as a function of the height of the potential barrier, $\Delta E/k_BT$ (scaled with respect to the energy k_BT), for different values of β. For both transitions, MTPT shows an overall monotonic decay with an increase in the barrier height. The extent of this decay increases with the increase in the values of β. Lower values of β correspond to an increased heterogeneity of the environment, which hinders the motion of the riboswitch aptamer by restricting its structural motions, i.e., the "caging" effect[13,27,34] imparted by the viscoelasticity of the surrounding medium. A comparison of the MTPT for the unfold/fold transition of the riboswitch aptamer portrays that the magnitude of MTPT for the ligand bound state is almost ten times higher as compared to the ligand unbound state. Since adenine binding stabilizes the triple helix junction of the aptamer domain through increased secondary and/or tertiary interactions, the ligand bound aptamer takes a longer time to cross the potential barrier. Figures 9(a) and 9(b) show a comparison of the MTPT, $\bar{\tau}_{TPT}$, obtained from our theory [Eq. (16), for $\beta = 1$] with those of the constant force pulling SMD simulations (at 10 pN). The results of the theory agree with those of the SMD simulations for both without and with ligand binding of the riboswitch.

V. CONCLUSIONS

This work investigates the effect of ligand binding on the conformational transitions of the *add* A-riboswitch aptamer in viscoelastic cellular environments. The unfold/fold transition is described as a stochastic dynamics of a suitable reaction coordinate in an asymmetric bistable potential well within the tenets of the Generalized Langevin Equation (GLE), both in the presence and absence of the ligand. Steered Molecular Dynamics (SMD) simulations are also performed to probe the effect of ligand binding on the structural transitions of the aptamer. The results of the probability distribution, TPTs and MTPTs, are estimated to obtain an insight into the transition dynamics of the riboswitch. A comparative study of the distributions of TPT reveals that the transit times for the ligand bound riboswitch aptamer are higher than that of ligand unbound ones. The transition path time of the riboswitch aptamer follows a counterintuitive trend as it decreases with the increase in the heights of the potential barrier. MTPT of the riboswitch aptamer with and without ligand binding increases with an increase in the viscoelasticity of the surrounding environment, which retards the motion of the riboswitch aptamer due to the "caging" effect. The remarkable agreement between the results of our calculations (both from theory and simulation) with those of experimental and other theoretical studies suggests that our model is able to capture the essential features of the effect of ligand binding induced conformational transitions of the riboswitch aptamer.

SUPPLEMENTARY MATERIAL

See the supplementary material for the solution of the GLE and effective Fokker–Planck equation; calculation of the normalization constants; theoretical and simulation results at different values of β and forces, respectively; PMF profiles vs the extension plots for the SMD simulations with implicit and explicit Mg^{2+} ions; and snapshots and multimedia files of the unfolding events of the riboswitch aptamer compiled from the SMD simulations.

ACKNOWLEDGMENTS

The authors gratefully acknowledge FRP Grant-IoE (No. IoE/FRP/PCMS/2020/27) for financial support and SCFBio (IIT, Delhi) for providing adequate supercomputing facility. Shivangi Sharma acknowledges UGC, India (Grant No. Schs/SRF/139/F-193/2012-13), and Vishal Singh acknowledges CSIR, India (Grant No. 09/045(1410)/2016/EMR-I), for providing financial assistance in the form of SRF.

DATA AVAILABILITY

The data that support the findings of this study are available within the article and its supplementary material.

REFERENCES

[1] K. Neupane, H. Yu, D. A. N. Foster, F. Wang, and M. T. Woodside, "Single-molecule force spectroscopy of the add adenine riboswitch relates folding to regulatory mechanism," Nucleic Acids Res. **39**, 7677–7687 (2011).
[2] V. Kumar, T. Endoh, K. Murakami, and N. Sugimoto, "Dehydration from conserved stem regions is fundamental for ligand-dependent conformational transition of the adenine-specific riboswitch," Chem. Commun. **48**, 9684–9686 (2012).
[3] S. Warhaut, K. R. Mertinkus, P. Höllthaler, B. Fürtig, M. Heilemann, M. Hengesbach, and H. Schwalbe, "Ligand-modulated folding of the full-length adenine riboswitch probed by NMR and single-molecule FRET spectroscopy," Nucleic Acids Res. **45**, 5512–5522 (2017).
[4] W. J. Greenleaf, K. L. Frieda, D. A. N. Foster, M. T. Woodside, and S. M. Block, "Direct observation of hierarchical folding in single riboswitch aptamers," Science **319**, 630–633 (2008).
[5] D. B. Ritchie and M. T. Woodside, "Probing the structural dynamics of proteins and nucleic acids with optical tweezers," Curr. Opin. Struct. Biol. **34**, 43–51 (2015).
[6] W. J. Greenleaf, M. T. Woodside, and S. M. Block, "High-resolution, single-molecule measurements of biomolecular motion," Annu. Rev. Biophys. Biomol. Struct. **36**, 171–190 (2007).
[7] K. C. Neuman and A. Nagy, "Single-molecule force spectroscopy: Optical tweezers, magnetic tweezers and atomic force microscopy," Nat. Methods **5**, 491 (2008).
[8] H. A. Heus, E. M. Puchner, A. J. van Vugt-Jonker, J. L. Zimmermann, and H. E. Gaub, "Atomic force microscope-based single-molecule force spectroscopy of RNA unfolding," Anal. Biochem. **414**, 1–6 (2011).
[9] J.-C. Lin and D. Thirumalai, "Relative stability of helices determines the folding landscape of adenine riboswitch aptamers," J. Am. Chem. Soc. **130**, 14080–14081 (2008).
[10] K. Neupane, D. A. N. Foster, D. R. Dee, H. Yu, F. Wang, and M. T. Woodside, "Direct observation of transition paths during the folding of proteins and nucleic acids," Science **352**, 239–242 (2016).
[11] K. Neupane, D. B. Ritchie, H. Yu, D. A. Foster, F. Wang, and M. T. Woodside, "Transition path times for nucleic acid folding determined from energy-landscape analysis of single-molecule trajectories," Phys. Rev. Lett. **109**, 068102 (2012).

[12]K. Neupane, N. Q. Hoffer, and M. Woodside, "Measuring the local velocity along transition paths during the folding of single biological molecules," Phys. Rev. Lett. **121**, 018102 (2018).
[13]S. Chaudhury and D. E. Makarov, "A harmonic transition state approximation for the duration of reactive events in complex molecular rearrangements," J. Chem. Phys. **133**, 034118 (2010).
[14]R. Satija and D. E. Makarov, "Generalized Langevin equation as a model for barrier crossing dynamics in biomolecular folding," J. Phys. Chem. B **123**, 802–810 (2019).
[15]R. Satija, A. Das, and D. E. Makarov, "Transition path times reveal memory effects and anomalous diffusion in the dynamics of protein folding," J. Chem. Phys. **147**, 152707 (2017).
[16]W. K. Kim and R. R. Netz, "The mean shape of transition and first-passage paths," J. Chem. Phys. **143**, 224108 (2015).
[17]A. M. Berezhkovskii, L. Dagdug, and S. M. Bezrukov, "Peculiarities of the mean transition path time dependence on the barrier height in entropy potentials," J. Phys. Chem. B **124**, 2305–2310 (2020).
[18]D. E. Makarov, "Interplay of non-Markov and internal friction effects in the barrier crossing kinetics of biopolymers: Insights from an analytically solvable model," J. Chem. Phys. **138**, 014102 (2013).
[19]R. Kubo, M. Toda, and N. Hashitsume, *Statistical Physics II: Nonequilibrium Statistical Mechanics* (Springer-Verlag, Berlin, Heidelberg, 1985), Vol. 31.
[20]R. Zwanzig, *Nonequilibrium Statistical Mechanics* (Oxford University Press, 2001).
[21]R. K. Montange and R. T. Batey, "Structure of the *S*-adenosylmethionine riboswitch regulatory mRNA element," Nature **441**, 1172 (2006).
[22]R. P. Mondescu and M. Muthukumar, "Statistics of an ideal polymer in a multistable potential: Exact solutions and instanton approximation," J. Chem. Phys. **110**, 12240–12249 (1999).
[23]M. O. Hongler and W. M. Zheng, "Exact solution for the diffusion in bistable potentials," J. Stat. Phys. **29**, 317–327 (1982).
[24]M. O. Hongler and W. M. Zheng, "Exact results for the diffusion in a class of asymmetric bistable potentials," J. Math. Phys. **24**, 336–340 (1983).
[25]H. Buchholz, *The Confluent Hypergeometric Function: With Special Emphasis on its Applications* (Springer Science & Business Media, 2013), Vol. 15.
[26]A. P. Manuel, J. Lambert, and M. T. Woodside, "Reconstructing folding energy landscapes from splitting probability analysis of single-molecule trajectories," Proc. Natl. Acad. Sci. U. S. A. **112**, 7183–7188 (2015).
[27]S. Sharma and P. Biswas, "Conformational transitions of a DNA hairpin through transition path times," J. Stat. Mech.: Theory Exp. **2020**, 073411.
[28]S. Sharma and P. Biswas, "Hydration water dynamics around a protein surface: A first passage time approach," J. Phys.: Condens. Matter **30**, 035101 (2017).
[29]S. Sharma and P. Biswas, "Unusual dynamics of hydration water around motor proteins with long-ranged hydrodynamic fluctuations," Physica A **534**, 122045 (2019).
[30]R. Gorenflo and A. Kilbas, *Mittag–Leffler Functions, Related Topics and Applications* (Springer, Berlin, 2016).
[31]M. Abramowitz and I. A. Stegun, *Handbook of Mathematical Functions with Formulas, Graphs, and Mathematical Tables* (Dover, New York, 1964), Vol. 55.
[32]I. S. Gradshteyn and I. M. Ryzhik, *Table of Integrals, Series, and Products* (Academic Press, 2014).
[33]M. Caraglio, S. Put, E. Carlon, and C. Vanderzande, "The influence of absorbing boundary conditions on the transition path time statistics," Phys. Chem. Chem. Phys. **20**, 25676–25682 (2018).
[34]E. Medina, R. Satija, and D. E. Makarov, "Transition path times in non-Markovian activated rate processes," J. Phys. Chem. B **122**, 11400–11413 (2018).
[35]D. Janakiraman, "Transition path time distributions for Lévy flights," J. Phys. A: Math. Theor. **51**, 285001 (2018).
[36]A. M. Berezhkovskii, L. Dagdug, and S. M. Bezrukov, "Mean direct-transit and looping times as functions of the potential shape," J. Phys. Chem. B **121**, 5455–5460 (2017).
[37]A. V. Chechkin, R. Metzler, V. Y. Gonchar, J. Klafter, and L. V. Tanatarov, "First passage and arrival time densities for Lévy flights and the failure of the method of images," J. Phys. A: Math. Gen. **36**, L537–L544 (2003).
[38]D. Janakiraman, "Lévy flights in the presence of a point sink of finite strength," Phys. Rev. E **95**, 012154 (2017).
[39]B. W. Zhang, D. Jasnow, and D. M. Zuckerman, "Transition-event durations in one-dimensional activated processes," J. Chem. Phys. **126**, 074504 (2007).
[40]C. W. Gardiner, *Handbook of Stochastic Methods* (Springer, Berlin, 1985), Vol. 3.
[41]S. Redner, *A Guide to First-Passage Processes* (Cambridge University Press, 2001).
[42]J. C. Phillips, R. Braun, W. Wang, J. Gumbart, E. Tajkhorshid, E. Villa, C. Chipot, R. D. Skeel, L. Kalé, and K. Schulten, "Scalable molecular dynamics with NAMD," J. Comput. Chem. **26**, 1781–1802 (2005).
[43]A. Pérez, I. Marchán, D. Svozil, J. Sponer, T. E. Cheatham III, C. A. Laughton, and M. Orozco, "Refinement of the AMBER force field for nucleic acids: Improving the description of α/γ conformers," Biophys. J. **92**, 3817–3829 (2007).
[44]M. Zgarbová, M. Otyepka, J. Šponer, A. Mládek, P. Banáš, T. E. Cheatham III, and P. Jurečka, "Refinement of the Cornell *et al.* nucleic acids force field based on reference quantum chemical calculations of glycosidic torsion profiles," J. Chem. Theory Comput. **7**, 2886–2902 (2011).
[45]W. F. Van Gunsteren and H. J. C. Berendsen, "A leap-frog algorithm for stochastic dynamics," Mol. Simul. **1**, 173–185 (1988).
[46]P. T. X. Li, J. Vieregg, and I. Tinoco, Jr., "How RNA unfolds and refolds," Annu. Rev. Biochem. **77**, 77–100 (2008).
[47]H. S. Hayatshahi, C. Bergonzo, and T. E. Cheatham III, "Investigating the ion dependence of the first unfolding step of GTPase-associating center ribosomal RNA," J. Biomol. Struct. Dyn. **36**, 243–253 (2018).
[48]E. Carlon, H. Orland, T. Sakaue, and C. Vanderzande, "Effect of memory and active forces on transition path time distributions," J. Phys. Chem. B **122**, 11186–11194 (2018).
[49]M. Laleman, E. Carlon, and H. Orland, "Transition path time distributions," J. Chem. Phys. **147**, 214103 (2017).